Available online at www.sciencedirect.com
SCIENCE DIRECT®
Advances in Space Research 37 (2006) 770–786
ADVANCES IN SPACE RESEARCH (a COSPAR publication)
www.elsevier.com/locate/asr

Spatial and temporal scales of the Brazil–Malvinas Current confluence documented by simultaneous MODIS Aqua 1.1-km resolution SST and color images

Nicolas Barré, Christine Provost *, Martin Saraceno

LODYC, UMR 7617, CNRS, UPMC, IRD, MNHN, Université Pierre et Marie Curie, T 45-55, 4 Place Jussieu, 75252 Paris Cedex 05, France

Received 3 February 2005; received in revised form 5 September 2005; accepted 6 September 2005

Abstract

The moderate resolution imaging spectroradiometer (MODIS) on board the Aqua satellite measures visible and infrared radiation in 36 wavebands, providing simultaneous images of sea-surface temperature (SST) and chlorophyll-*a* (chl-*a*) concentration in the upper meters of the sea. For the first time, truly synoptic SST and chl-*a*- concentration images are available. These images are daily and of 1.1-km resolution.

The strong contrasts in sea-surface temperature and surface chlorophyll-*a* concentration over the southwest Atlantic make satellite infrared and color images particularly appropriate tools for studying the Brazil–Malvinas (B/M) Current confluence. We examine two years (July, 2002–June, 2004) of Aqua/MODIS infrared and color images to document the precise structure of the B/M confluence simultaneously in SST and chl-*a*.

We first compared MODIS weekly data with simultaneous independent satellite data. Spatial and temporal distributions are similar for both SST and color. Differences between MODIS and SeaWiFS (sea-viewing wide field-of-view sensor) are large in pigment-rich regions along the coast and shelf. Here, we focused on the offshore region where differences are small.

For each season, exceptionally cloud-free 1.1-km resolution MODIS images showed two thermal fronts, one corresponding to the Brazil Current's southernmost limit, the other, to the Malvinas Current's northernmost limit. These two fronts remained quite close to each other (within 50 km) and were separated by water with an SST and chl-*a* concentration typical of the continental shelf waters. In spring, the water rich in chl-*a* from the platform is squeezed between the two currents and entrained away from the coast in between the two thermal fronts. In the frontal region, SST gradient maxima trace the contour of the chl-*a*-rich water.

Enlargements of the frontal region and of the turbulent region downstream of the frontal collision are presented and analyzed. MODIS documents in an unprecedented way the SST and chl-*a* filaments as they are distorted and mixed by meso- and sub-mesoscale structures in the strain-dominated region of the B/M confluence. It is suggested that a substantial part of the chl-*a* local maximum in the Malvinas return flow is of continental-shelf origin.

Keywords: Oceanic color; Ocean fronts; Eddies and filaments; MODIS

1. Introduction

The region of the South Atlantic where the warm, high-salinity, southward-flowing Brazil Current (BC) encounters the cold, low-salinity, northward-flowing Malvinas Current (MC) is called the Brazil–Malvinas Confluence (Fig. 1(a)). It is off the coast of Argentina and Uruguay, between 30°S and 50°S and 40°W and 60°W. After meeting, the BC and MC leave the coast. The main flow of the MC describes a sharp loop forming the Malvinas Return Flow (MRF). In the southwest Atlantic two strong oceanic fronts are present: the Subtropical Front (STF), sometimes called the Brazil Current Front (BCF), and the Subantarctic Front (SAF) (Fig. 1(a)). The BCF is a boundary of the BC, and the SAF, similarly, for the MC.

* Corresponding author. Tel.: +33 14 427 3481; fax: +33 14 427 7159.
E-mail address: cp@lodyc.jussieu.fr (C. Provost).

0273-1177/$30 © 2006 Published by Elsevier Ltd on behalf of COSPAR.
doi:10.1016/j.asr.2005.09.026

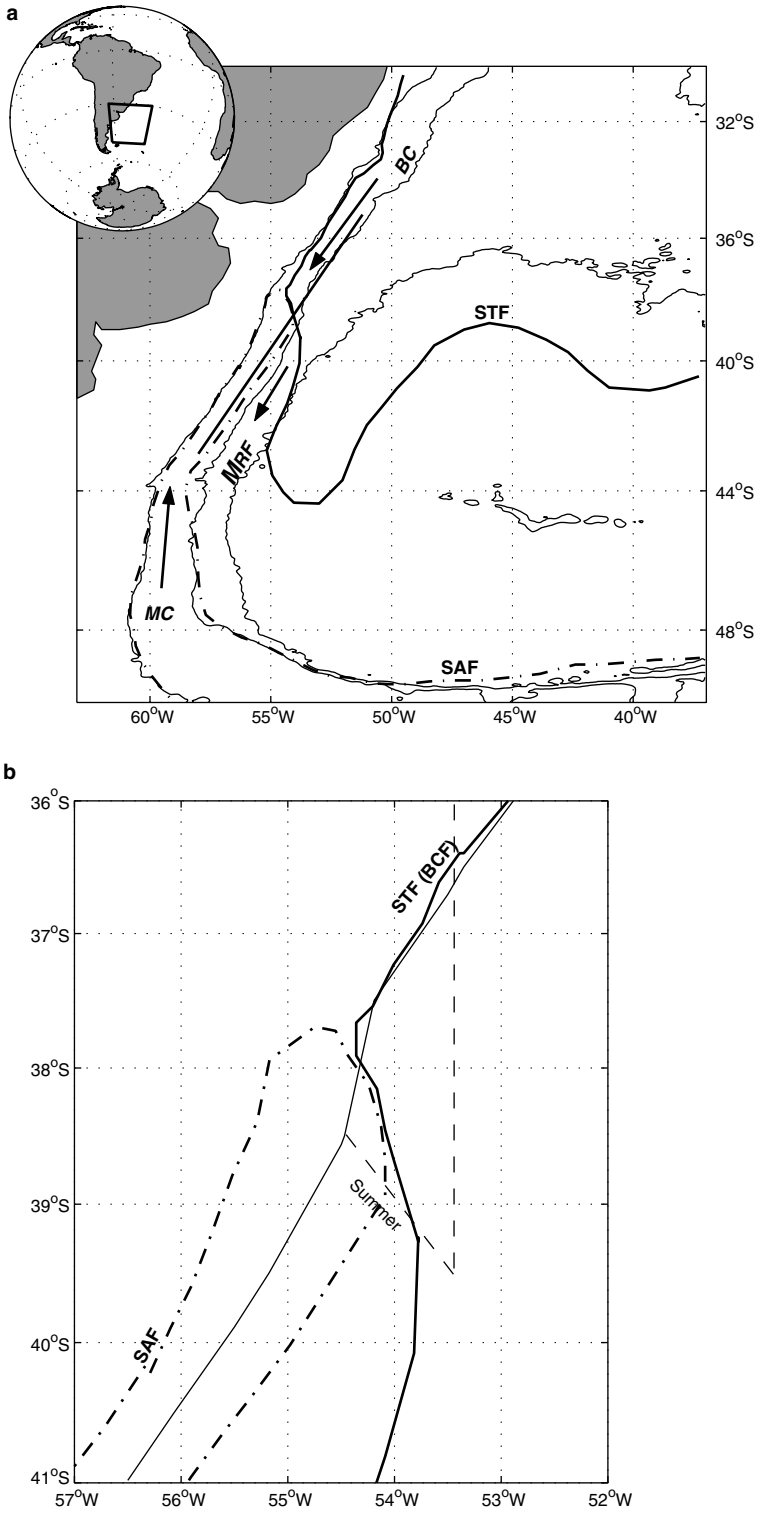

Fig. 1. (a) Diagram of the major fronts and currents in the southwest Atlantic. The confluence of the Malvinas Current (MC) and the Brazil Current (BC) occurs near 38°S. The mean position of the subtropical front (STF, solid line) and the Subantarctic front (SAF, dash-dotted line) are from Saraceno et al. (2004). *MRF* Malvinas Return Flow. Isobaths at 300, 3000, and 5000 m (from Smith et al., 1994) are shown. The along-shelf section (solid black line) is used to plot the Hovmoller diagram of Fig. 3. (b) Schematic position of the surface fronts in the B/M confluence region: STF thick line, SAF dash-dotted line. The thin line is the 1000-m isobath.

The contrasts in sea-surface temperature, in chlorophyll-*a* concentration and the local maximum in eddy kinetic energy make satellite infrared (IR) imagery (e.g., Olson et al., 1988; Provost et al., 1992; Saraceno et al., 2004), color imagery (Saraceno et al., 2005) and satellite altimetry (e.g., Provost and Le Traon, 1993; Goni and Wainer,

2001) particularly appropriate tools for studying the confluence. The satellite data provide valuable information in this area, which, like most of the southern hemisphere oceans, has few in situ time-series observations.

Using advanced very-high-resolution radiometer (AVHRR) data from 1981 to 1987, and tracing isotherms on SST images, Olson et al. (1988) estimated that the SAF separates from the continental shelf break at 38.6 ± 0.9°S; that is, 2° south of the STF separation point. They found that the range of migration of the separation point for the BC and MC is about 900 km, which is quite large compared to other western boundary current systems. The associated variability occurs at an annual time-scale, with an important interannual component. The variation in the latitude of separation of both currents from the coast has been a subject of much investigation and debate based on theories and models (e.g., Agra and Nof, 1993; Matano, 1993; Lebedev and Nof, 1996, 1997; Gan et al., 1998). Two characteristics of the separation have been investigated: a mean position of the separation point nearly 15°N of the zero of the wind stress curl line and a seasonal migration of the separation point with a poleward shift during the austral summer. These theoretical works have underscored the role of the dynamics of two colliding jets. Indeed, the MC has a mean transport of 40–45 Sv, similar to that of the BC, which could explain why the BC leaves the coast 15° North of the zero wind stress curl (Vivier and Provost, 1999). The important interannual variability of the MC transport could have an impact on the interannual migrations of the BC/MC confluence. However, the MC transport variability does not have any annual component (Vivier and Provost, 1999) and therefore cannot explain the annual migrations of the confluence observed by Olson et al. (1988) (Vivier and Provost, 1999).

Using a combination of altimetric and thermocline-depth data, Goni and Wainer (2001) found that in 1993–1998 the separation of the STF from the shelf break occurred on average at 38.5 ± 0.8°S, which is 2° south of the position described by Olson et al. (1988), and presents little migration.

Saraceno et al. (2004) analyzed surface thermal fronts using nine years (1987–1995) of 4-km-resolution 5-day composite images from AVHRR data. They detected fronts using a gradient-based edge detector. They found that the STF and SAF merged into a single front at the meeting of the two currents, and that this front did not present large seasonal north–south excursions. The meeting-point front pivoted seasonally around a fixed point at approximately 39.5°S, 53.5°W, changing its orientation from N–S during most of the year to NW–SE in summer. Consequently, on average, the front intersects the 1000-m isobath at 38.30°S in summer and north of 37°S in winter (Fig. 1(b)). No significant interannual variability in the front position is observed.

Saraceno et al. (2005) then examined the space–time distribution of chlorophyll-*a* in the southwest Atlantic using six years (1998–2003) of sea-surface color images (9-km resolution, 8-day composites) from SeaWiFS. The Brazil–Malvinas front corresponds to high chlorophyll-*a* concentrations compared to the chlorophyll-*a*-poor Malvinas and Brazil Currents. The location of the chlorophyll-*a* maximum matches the location of the SST gradient maximum associated with the collision front. The results found with SST were confirmed: the BC and MC meet in a single front which remains at the same place throughout the year, with a N–S orientation, except in summer when it tends to shift to NW–SE.

Here, we have investigated the precise structure the B/M front using Level-2 resolution (1.1-km and 1-day) simultaneous SST and color images provided by the moderate resolution imaging spectroradiometer (MODIS) on board the Aqua satellite since 4 May, 2002. The paper is organized as follows. After a Section 2 on data and methods, we compare Aqua/MODIS Level-3 data (IR and visible) with simultaneous independent Level-3 satellite data (advanced microwave scanning radiometer for EOS [AMSR-E] for SST, and SeaWiFS for color). Differences between the data sets are identified and discussed. The comparison suggests that Aqua/MODIS can be used quantitatively over deep waters. In Section 3, we analyze a few Aqua/MODIS 1.1-km resolution simultaneous cloud-free images of SST and chlorophyll-*a* concentration for each season. We focus on the frontal region and on the turbulent region downstream of the front. Variations on short time scales are documented by examining successive images. A summary, discussion and perspective Section 4 concludes the paper.

2. Data and methods

2.1. Data sources for inter-comparisons

We used data from two independent space-borne ocean-color sensors: the sea-viewing wide field-of-view sensor (SeaWiFS), and the moderate resolution imaging spectroradiometer (MODIS) from the Aqua satellite. The SeaWiFS instrument has been in continuous operation since September 1997, whereas the Aqua/MODIS instrument has been collecting data only since 4 May, 2002. With the recent reprocessing of the data sets of both instruments, there are now almost two years of consistently processed, contemporaneous MODIS and SeaWiFS data available through the Goddard distributed active archive (DAAC). To compare chlorophyll-*a* concentrations derived from SeaWiFS and MODIS data for the Brazil–Malvinas confluence, we used standard Level-3 weekly data products available from the DAAC for both sensors (9-km resolution for SeaWiFS and 4.6-km for MODIS). We examined seasonal means over the region (Fig. 2). Temporal variation in SST along a section perpendicular to the Brazil–Malvinas front is shown in Fig. 4.

For SST comparisons, we used data from two independent sensors carried on board the Aqua satellite: MODIS

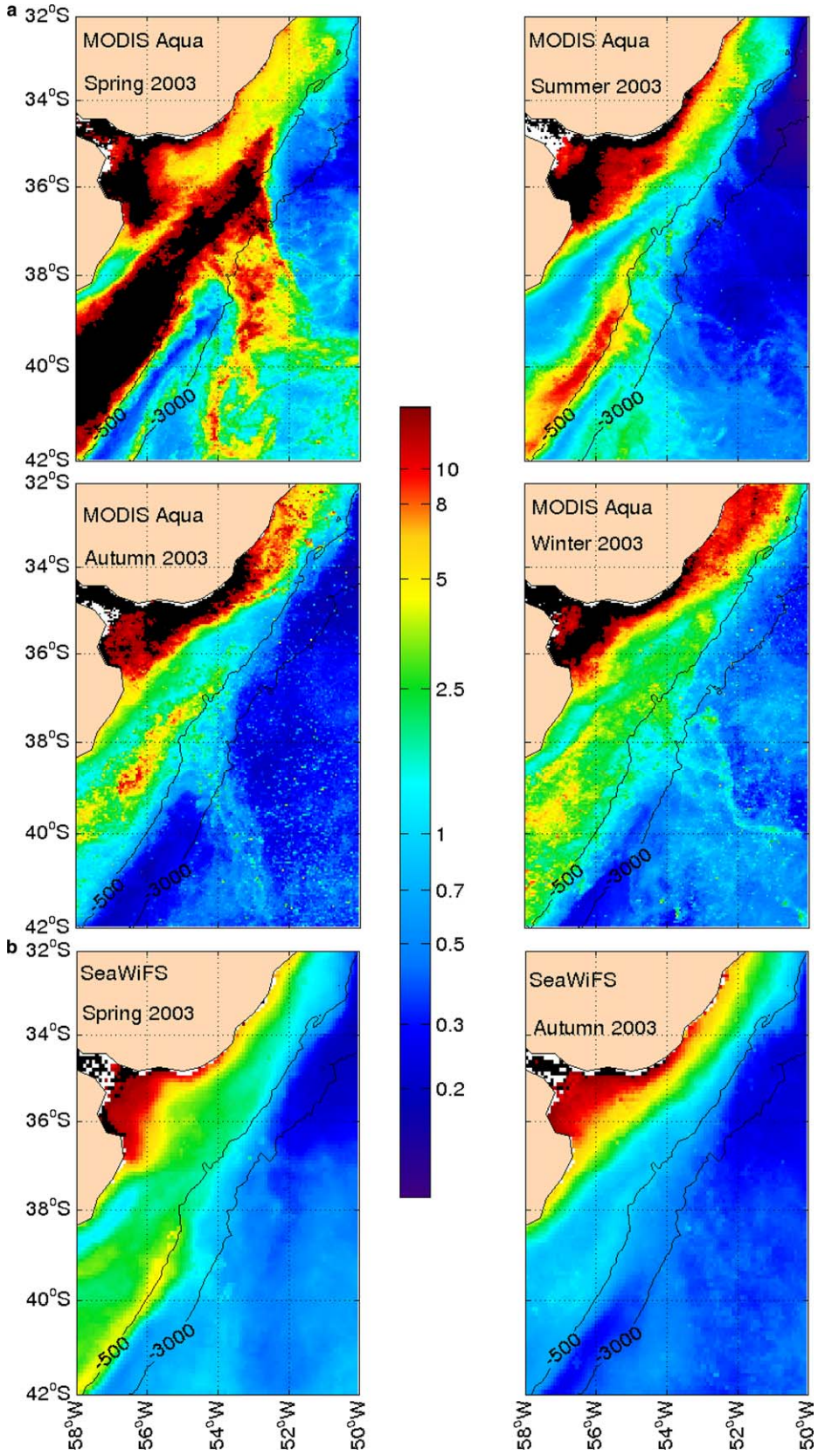

Fig. 2. Seasonal averages of chlorophyll-*a* concentration from MODIS and SeaWiFS data for the year 2003; both are Level-3 data. MODIS has a 4.6-km resolution and SeaWiFS, a 9-km resolution. The color scale (in mg/m^3) is the same. (a) The four seasons are presented for the MODIS data: austral summer (January, February, March); autumn (April, May, June); winter (July, August, September); spring (October, November, December). (b) Two seasons are shown for the SeaWiFS data: spring and autumn.

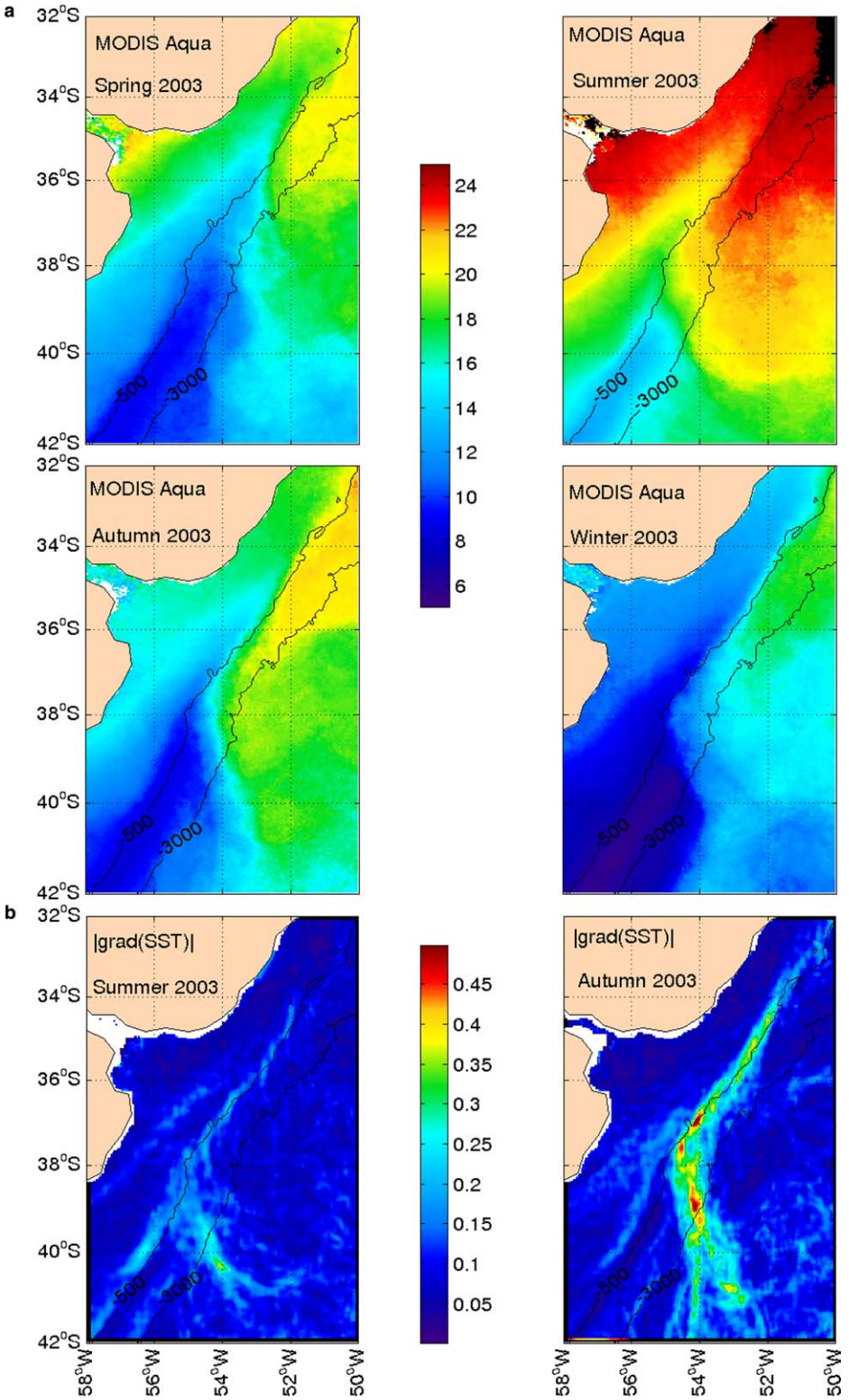

Fig. 3. Seasonal averages of SST and SST gradients derived from the MODIS data and from the optimally interpolated products, AMSR-E + TMI for the year 2003. Both are Level-3 weekly averaged data. MODIS has a 4.6-km resolution and AMSR-E + TMI, a quarter-of-a-degree (~25 km) resolution. (a) Seasonal averages (in °C) of MODIS SST. (b) MODIS SST gradients (in °C/km) in summer and autumn. (c) Seasonal averages (in °C) of SST from AMSR-E + TMI in summer and autumn. (d) AMSR-E + TMI SST gradients (in °C/km) in summer and autumn.

and Advanced Microwave Scanning Radiometer for EOS (AMSR-E). The latter is the first microwave radiometer capable of accurately measuring global through-cloud SSTs. The data sets are Level-3 weekly MODIS SST (4.6-km resolution) and weekly composites of Level-3 AMSR-E SST products with a quarter-of-a-degree (~25 km) resolution

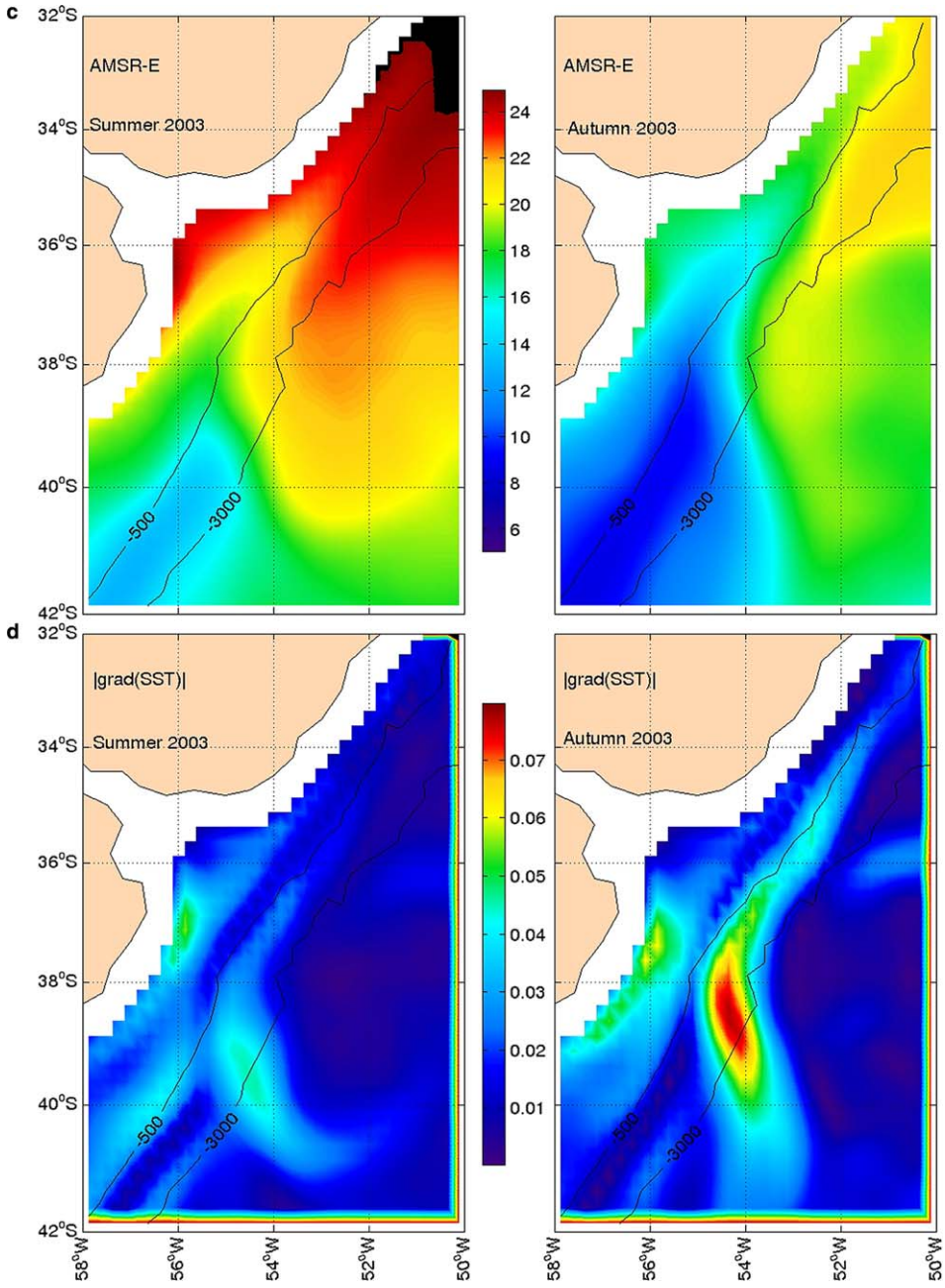

Fig. 3. (*continued*)

provided by Remote Sensing Systems (http://www.ssmi.com/sst/microwave_oi_sst_data_description.html). Maps of seasonal SST averages for the year 2003 are reproduced in Fig. 3. Gradient images were computed and used to detect fronts and to estimate the probability of a front being present, as in Saraceno et al. (2004) (see Fig. 5).

2.2. Production and analysis of 1.1-km-resolution MODIS SST and chlorophyll-a images

We first examined MODIS Level-3 daily browse data on the SeaWiFS data server (http://oceancolor.gsfc.nasa.gov/SeaWiFS.html) for the period July, 2002–June, 2004, in order to select the dates for which the B/M front was cloud-free or only partly masked. Of the 660 images examined, 170 were selected. The number of selected images varied with season (27 in winter, 65 in spring, 58 in summer, 20 in autumn) and the first year, from July, 2002 to June, 2003, appeared less cloudy than the second, from July, 2003 to June, 2004 (Fig. 6). Thus, a data set of 170 images (Level-3, daily, 4.6-km-resolution) for SST and color were extracted from the region (50°–58°W, 32°–42°S) and calibrated.

Then, we selected one subset of images for each season for which we produced 1-km-resolution images. We

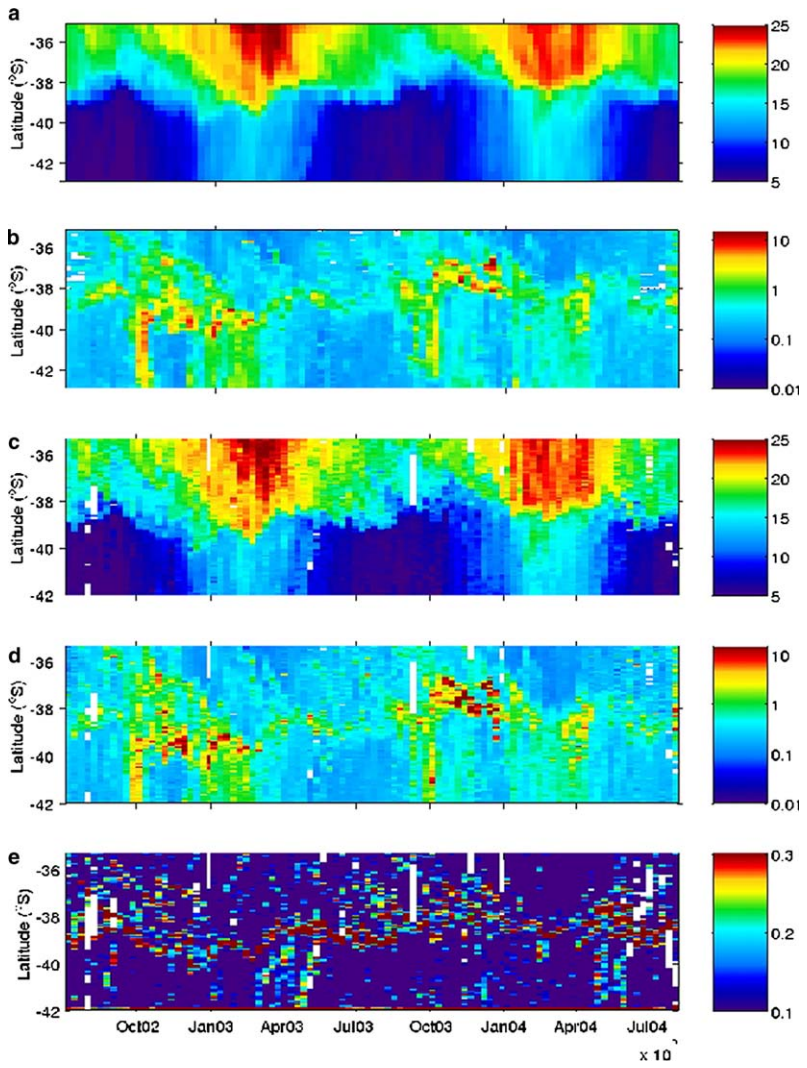

Fig. 4. Temporal variation in various parameters along a section perpendicular to the B/M front; *x*-axis is time, *y*-axis is latitude. All parameters have a time resolution of one week. (a) SST (in °C) from AMSR-E+TMI (quarter-of-a-degree resolution). (b) Chlorophyll-*a* concentration (in mg/m^3) derived from SeaWiFS data (9-km resolution). (c) SST (in °C) from MODIS (4.6-km resolution). (d) Chlorophyll-*a* concentration (in mg/m^3) derived from MODIS data. (e) SST gradient (in °C/km) from MODIS data.

downloaded the corresponding Level-2 MODIS data from the SeaWiFS website. The zone of interest was extracted and the projection was performed using the SeaWiFS Data Analysis System (SeaDAS – http://seadas.gsfc.nasa. gov/). For each image, an SST gradient-amplitude image was computed, as described in Saraceno et al. (2004).

One 1.1-km resolution image from each season is shown in Fig. 7 and an enlargement of the frontal region is shown in Fig. 8. Sections of the various parameters (Chl-*a*, SST, grad SST) across the B/M front were produced for each season (Fig. 9). An enlargement of the turbulent region downstream of the front in spring and a section across this region further document the spatial relationships between Chl-*a*, SST and SST gradients (Figs. 10 and 11). Differences between successive images document the temporal variability at short time-scales for both SST and chlorophyll-*a* for one pair of summer images (Fig. 11). The temperature/chlorophyll-*a* scatter plots allowed discussion of the origin of the water masses, apparent growth rates and possible relationships between temperature and chlorophyll-*a* variations (Fig. 12).

3. Weekly data – comparison of chlorophyll-*a* and SST data from MODIS with other satellite products

3.1. Seasonal maps

3.1.1. Color

On average the seasonal mean over the region obtained for the year 2003 by MODIS and by SeaWiFS exhibit similar patterns (Fig. 2): very high values in the Río de la Plata and along the Uruguayan coast in all seasons; high values along the shelf break, with a spectacular bloom in spring; low values over the Brazil and Malvinas Currents; moder-

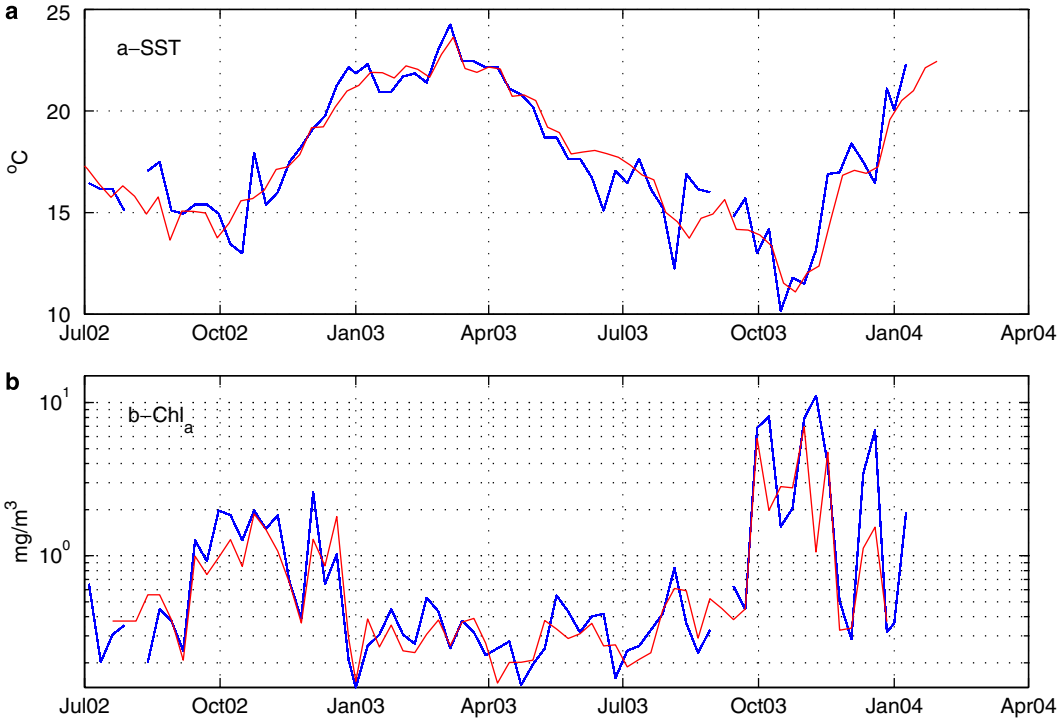

Fig. 5. (a) Time-series of SST from MODIS (blue) and AMSR-E (red) at 53.2°W, 37.5°S, in the region of the B/M front in the section plotted in Fig. 3. SST mean values (18.2 °C) and standard deviation (±3.2 °C) are similar for the MODIS and the AMSR-E data; the standard deviation of the difference is ±2.4 °C. (b) Time-series of chlorophyll-*a* concentration from MODIS (blue) and SeaWiFS (red) at 53.2°W, 37.5°S. Mean values: SeaWiFS, 0.83 mg/m^3; MODIS, 1.26 mg/m^3; standard deviations: SeaWiFS, ±1.21 mg/m^3; MODIS ±2.12 mg/m^3; standard deviation of the difference ±1.91 mg/m^3.

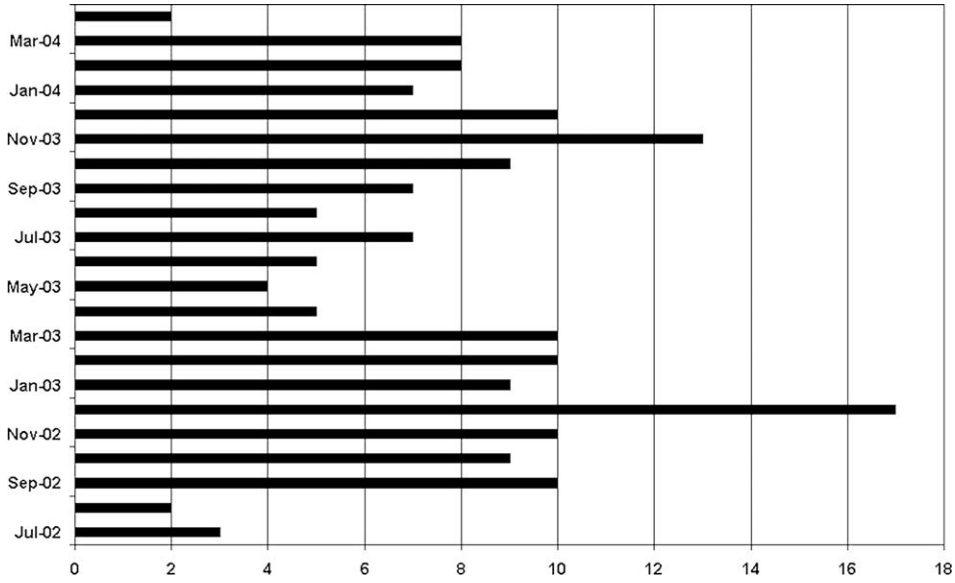

Fig. 6. Histogram of the number of usable images (i.e., with a limited amount of cloud cover), by month.

ate to high values in the frontal region; and high seasonally dependent values (low in autumn, maximum in spring) on the eastern flank of the MC, known as the Malvinas Return Front (MRF). However, MODIS images are much more contrasted than SeaWiFS images. Low values (<1 mg/m^3) are similar in amplitude and distribution; high values are much higher in MODIS. In particular, MODIS and SeaWiFS values over the continental shelf, the shelf break and the front often differ by more than a factor of 3. The turbid waters of the Río de la Plata showed the highest variability and complexity in optical properties, while the offshore waters have the lowest variability and

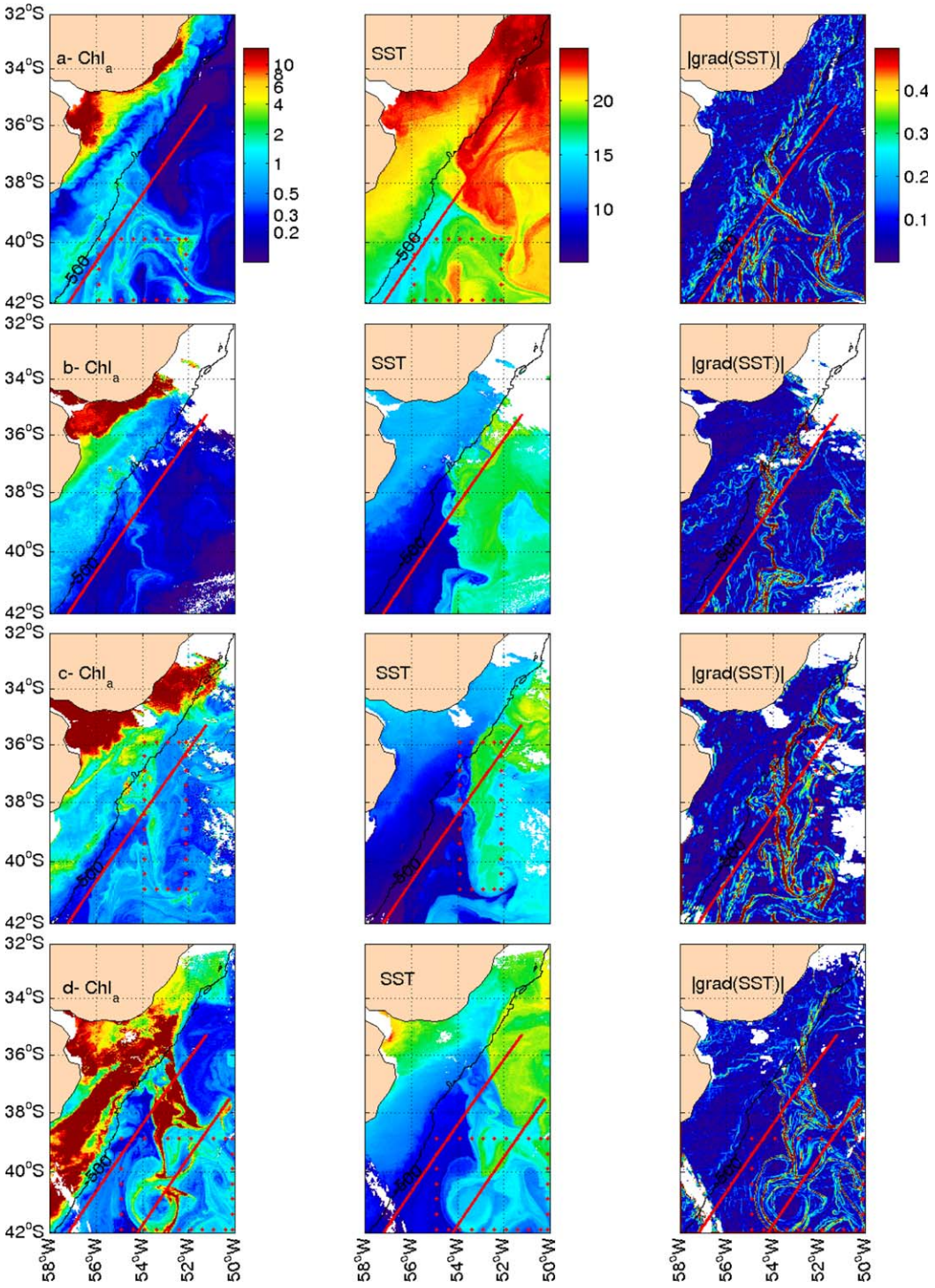

Fig. 7. 1.1-km resolution MODIS images for Chl-*a*, SST and SST gradients for: (a) Summer: 5 March, 2004; the dotted box region is enlarged in Fig. 11(a). (b) Autumn: 17 June, 2003. (c) Winter: 22 August, 2002; the dotted box region is enlarged in Fig. 8. (d) Spring: 27 October, 2003; the dotted box region is enlarged in Fig. 10. (Units are: °C for SST, mg/m^3 for Chl-*a* concentration and °C/km for SST gradient). Red lines correspond to sections shown in Figs. 9 and 10.

complexity. SeaWiFS operational processing makes use of the OC4v4 algorithm, whereas MODIS makes use of OC3M (O'Reilly et al., 2000). Commonly used visible wavebands include 490/488 nm (SeaWiFS band 3 and MODIS band 10) and 555/551 nm (SeaWiFS band 5 and MODIS band 12). As turbidity increases, the selected maximum band migrates from shorter (blue) to longer (green) wavelengths (Werdel, 2004). For the most turbid water, OC4v4 selects 510 nm, whereas OC3M remains at 488 nm. This leads to differing estimates of chlorophyll-*a* concentration in turbid water. Thus, we did not examine chlorophyll-*a* concentration along the coast and over the

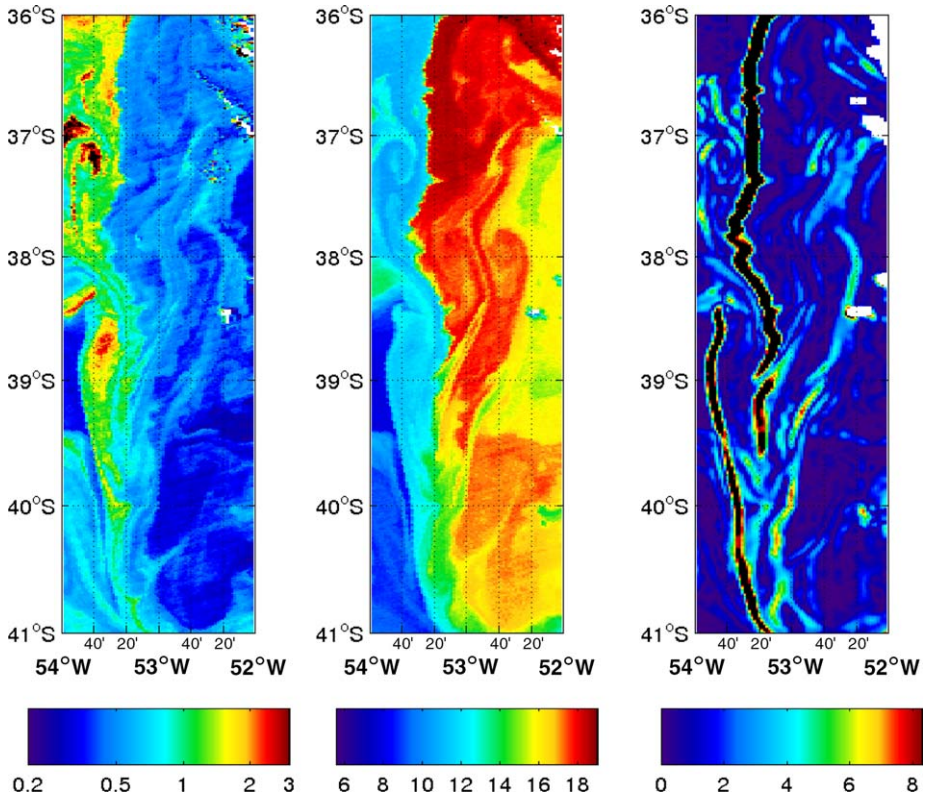

Fig. 8. Enlargement of the B/M front region in winter (22 August, 2002). From left to right: Chl-*a* concentration in mg/m^3; SST in °C; SST gradient in °C/km. MODIS 1.1-km-resolution images.

continental shelf. Rather we focused on the open ocean, offshore from the 500-m isobath.

The difference in spatial resolution between the images used to produce the seasonal means (4.6-km for MODIS and 9-km for SeaWiFS) resulted in significantly more detailed features in the averages from MODIS than in those from SeaWiFS. The difference in chlorophyll-*a* values between MODIS and SeaWiFS in the open ocean are further examined in Section 3.2.

3.1.2. SST

MODIS seasonal SST maps (Fig. 3) were similar both in distribution and amplitude to those obtained from AMSR-E (Fig. 3). MODIS SST gradient maps (Fig. 3) compared well to those derived from AMSR-E in spatial distribution. Mean gradients amplitudes derived from AMSR-E were about twice as small as those derived from MODIS; this is due to the difference in spatial resolution between the two data sets (4.6 vs. 25-km).

3.2. Temporal variation along a section perpendicular to the B/M front

The temporal variation in chlorophyll-*a* concentration and SST along the section perpendicular to the BM front (defined in Fig. 1) showed the good agreement between MODIS and AMSR-E data for SST and between MODIS and SeaWiFS data for chlorophyll-*a* concentration (Fig. 4). Fig. 4 also illustrates the spatial match between the SST front, as defined by the SST gradient maximum, and the chlorophyll-*a* maximum in these weekly averaged low-resolution images. The section roughly followed the 1000-m isobath. It confirmed a seasonal excursion of about 300 km in the frontal signature both for SST and color, as described in Saraceno et al. (2004, 2005).

Time-series of SST and chlorophyll-*a* concentrations for the location 37.62°S, 53.2°W, which corresponded to one pixel near the front on the section in Fig. 4, further illustrate the comparison between MODIS and AMSR-E/TMI for SST and between MODIS and SeaWiFS for color (Fig. 5). The two SST time-series have similar means (18.2 °C) and similar standard deviations (3.2 °C). Taking into account the uncertainty in pixel location, the difference in pixel size (4.6-km for MODIS and about 25-km for AMSR-E) and the small-scale features present in the region, the agreement in SST is very good. The chlorophyll-*a* concentration time-series was similar. The only significant difference occurred at high chlorophyll-*a* concentrations: MODIS values tended systematically to exceed SeaWiFS values (Fig. 5). The agreement is remarkable considering that the pixel size is not the same for SeaWiFS and MODIS (9 vs. 4.6 km) and that the point is in the frontal region where spatial gradients are large.

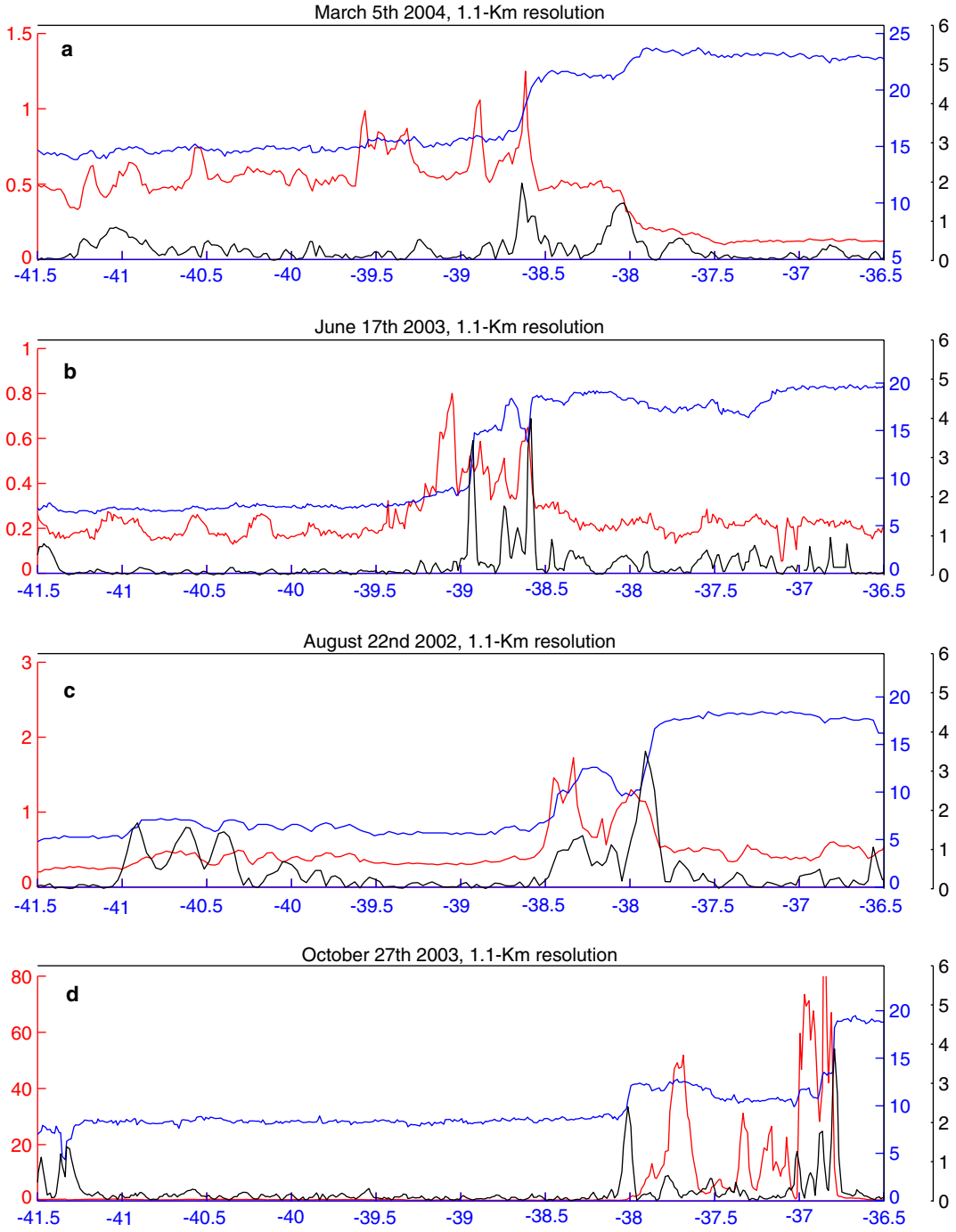

Fig. 9. Section across the B/M front for SST (blue, in °C), grad SST (black, in °C/km) and Chl-*a* (red, in mg/m^3) as a function of latitude. From top to bottom: on 5 March, 2004 (summer); on 17 June, 2003 (autumn); on 22 August, 2002 (winter); and on 27 October, 2003 (spring). The scale for Chl-*a* concentration is variable: 0–1.5 mg/m^3 in summer, 0–1 mg/m^3 in autumn, 0–3 mg/m^3 in winter, and 0–80 mg/m^3 in spring.

3.3. High-resolution simultaneous MODIS images of SST and chlorophyll-a concentration

3.3.1. General description

Instantaneous MODIS images at 1.1-km resolution for chlorophyll-*a* concentration, SST and SST gradients are given in Fig. 7 for the four seasons: summer (5 March, 2002), autumn (17 June, 2003), winter (22 August, 2003) and spring (27 October, 2003). These images were selected because of their exceptionally low cloud cover and because they preceded or followed another low-cloud-cover image, thus providing information about variation at short time-scales. These images reveal a wealth of structures at all scales in both SST and color (Fig. 7). We concentrated here on surface signals where the water depth exceeded 500 m.

We observed the change in orientation of the B/M front from N–S most of the year to NW–SE in austral

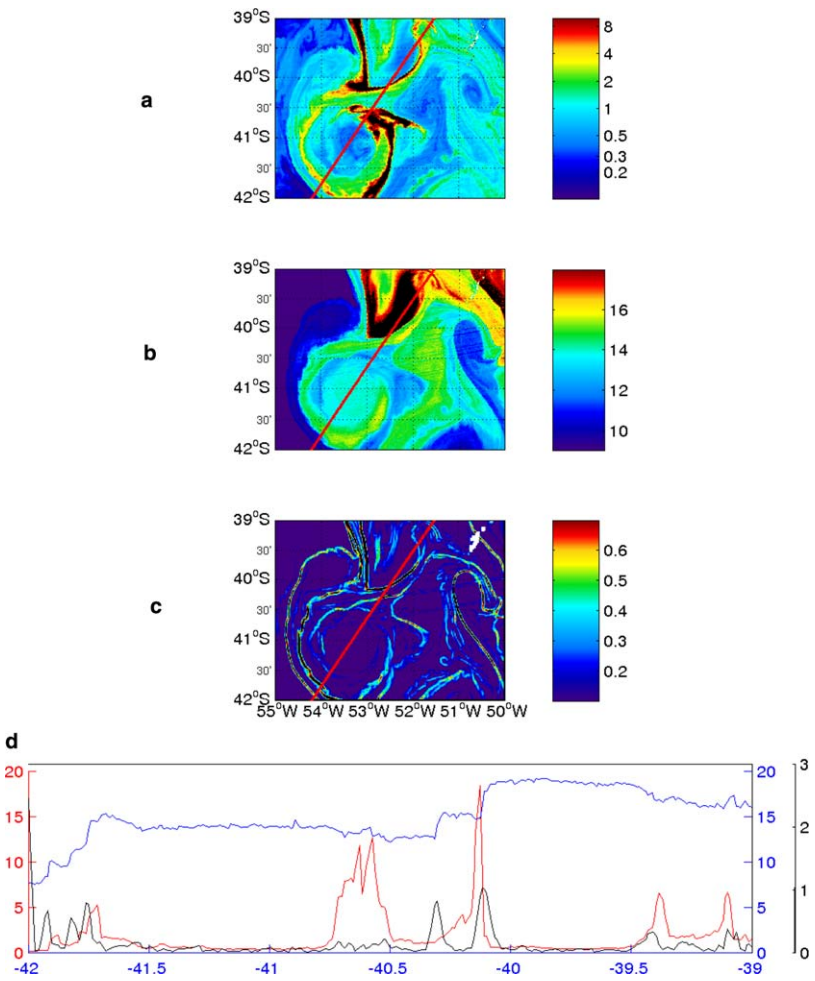

Fig. 10. Enlargement of the eddy-filled region downstream of the Brazil–Malvinas Current confluence on 27 October, 2003. (a) Chl-*a* concentration in mg/m^3. (b) SST in °C. (c) SST gradient in °C/km. (d) Section of SST (blue, in °C), SST gradients (black, in °C/km) and Chl-*a* concentration (red, in mg/m^3) as a function of latitude, corresponding to the red line in Fig. 10(a)–(c).

summer, in both SST and chlorophyll-*a*. The Brazil and Malvinas Currents both have low surface-chlorophyll-*a* concentrations. The confluence is marked by a local maximum in chlorophyll-*a* concentration. The images suggest horizontal entrainment and "stretching" of slope/shelf chlorophyll-*a*-rich water by the currents associated with B/M front. The strong influence of the currents is also apparent in the eddy and filament structures traced out by the chlorophyll-*a* and SST downstream of the B/M confluence. The images give the impression of a close connection between SST and the chlorophyll-*a* structures in all seasons and for all scales and types of structure. The links between SST and chlorophyll-*a* are documented further below, first examining space-scales, and then short time-scales.

3.3.2. Space-scales

To document space-scales, we made an enlargement of two areas: the B/M front in summer (Fig. 8) and the turbulent region downstream of the confluence in spring (Fig. 10). We also present two sections: one parallel to the isobaths and perpendicular to the B/M collision front (Fig. 9) in all seasons; and one farther offshore in the region dominated by meso- and sub-mesoscale structures downstream of the B/M front in spring (Fig. 11). (The sections are indicated in Fig. 7.)

3.3.2.1. The Brazil and Malvinas Current frontal region. The enlargement of the confluence image in winter (22 August, 2002) shows the close relationship between SST and chlorophyll-*a* (Fig. 8). The SST gradient maximum traces the contour of the chlorophyll-*a* maximum at the front. High chlorophyll-*a* concentrations were found on the southern side of the thermal front corresponding to the southern limit of the BC and northward of the thermal front corresponding to the northern limit of the MC. The narrow (up to 50 km wide) elongated region between the two fronts had temperature and chlorophyll-*a* concentrations typical of those of the continental shelf water (Fig. 7).

The surface water associated with the continental shelf was less saline than either the MC or the BC water. It was warmer than the MC and colder than the BC water and buoyant relative to both. The Malvinas Current water is denser than the Brazil Current water (Provost et al.,

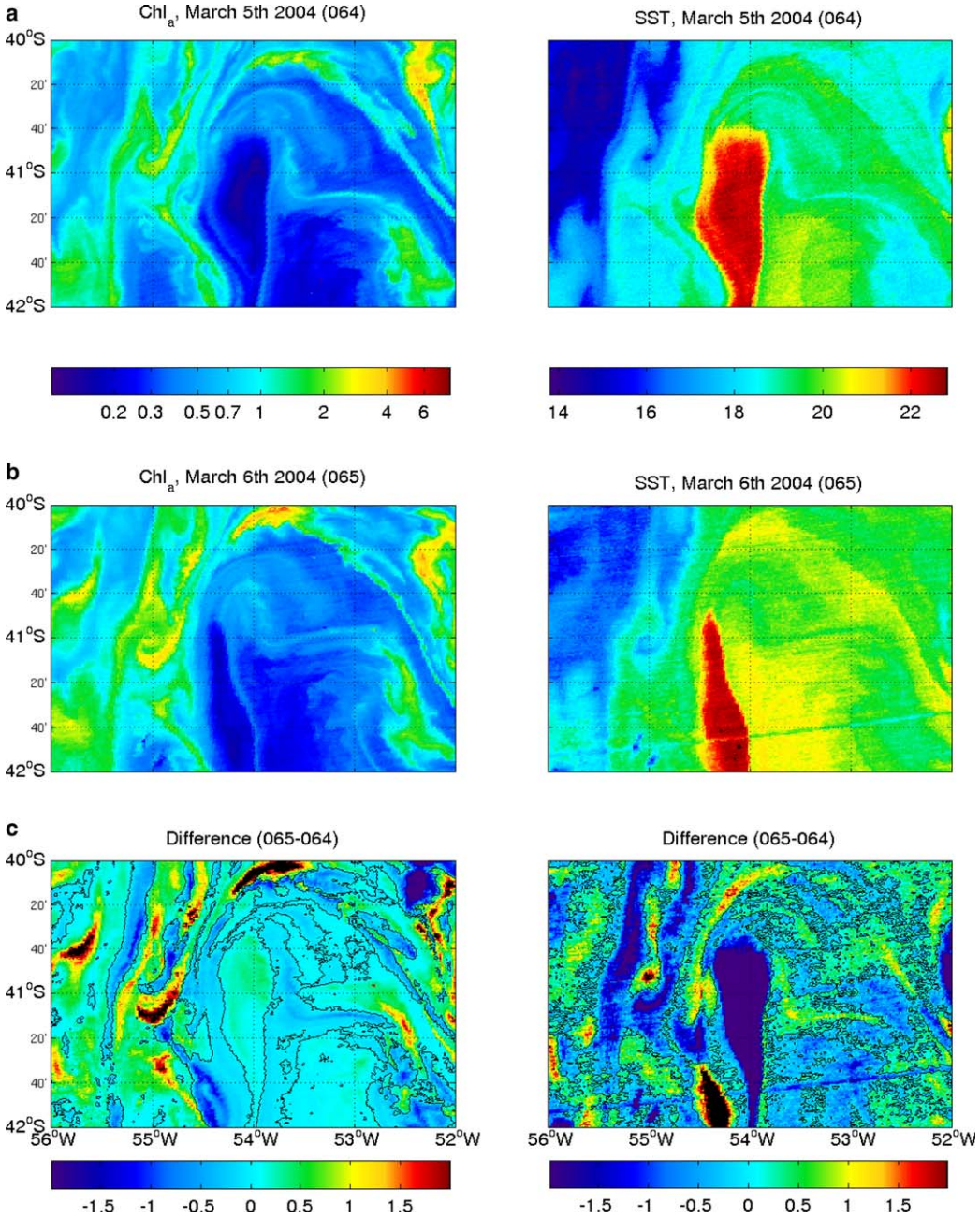

Fig. 11. Enlargement of Fig. 7(a) in the region downstream of the Brazil–Malvinas Current confluence. (a) Chl-*a* concentration (in mg/m^3) and SST (in °C) on 5 March, 2004. (b) Chl-*a* concentration (in mg/m^3) and SST (in °C) on 6 March, 2004. (c) Differences in Chl-*a* concentration (in mg/m^3) and in SST (in °C) between these two consecutive summer images.

1995): at the confluence part of the MC returns southwestward, and part of it sinks below the BC. The current along the front is extremely fast; speeds as high as 1.5 m/s have been reported (Vigan et al., 2000).

The image in Fig. 8 suggests that the light surface water from the continental shelf was entrained offshore by the current resulting from the confluence of the BC and the MC. Indeed, during a summer hydrographical cruise, Provost et al. (1996) observed very low-salinity (less than 32) surface water of continental-shelf origin in the frontal zone more than 300 km from the coast. This very light surface water squeezed between the northward-flowing MC and southward-flowing BC was entrained at the surface along the front away from the coast.

Sections across the B/M front in each season (Fig. 9) documented further the relationship between SST and chlorophyll-*a* at the front. The SST (in blue) shows two fronts between 39°S and 36.5°S on the section. The distance between the two thermal fronts did not exceed 0.5° in latitude (~50 km) except in the spring image where it reached 1° in latitude. The jumps in SST were larger in winter than in summer: this was due to the strong shallow seasonal thermocline that developed over the MC and reduced horizontal gradients (Provost et al., 1995).

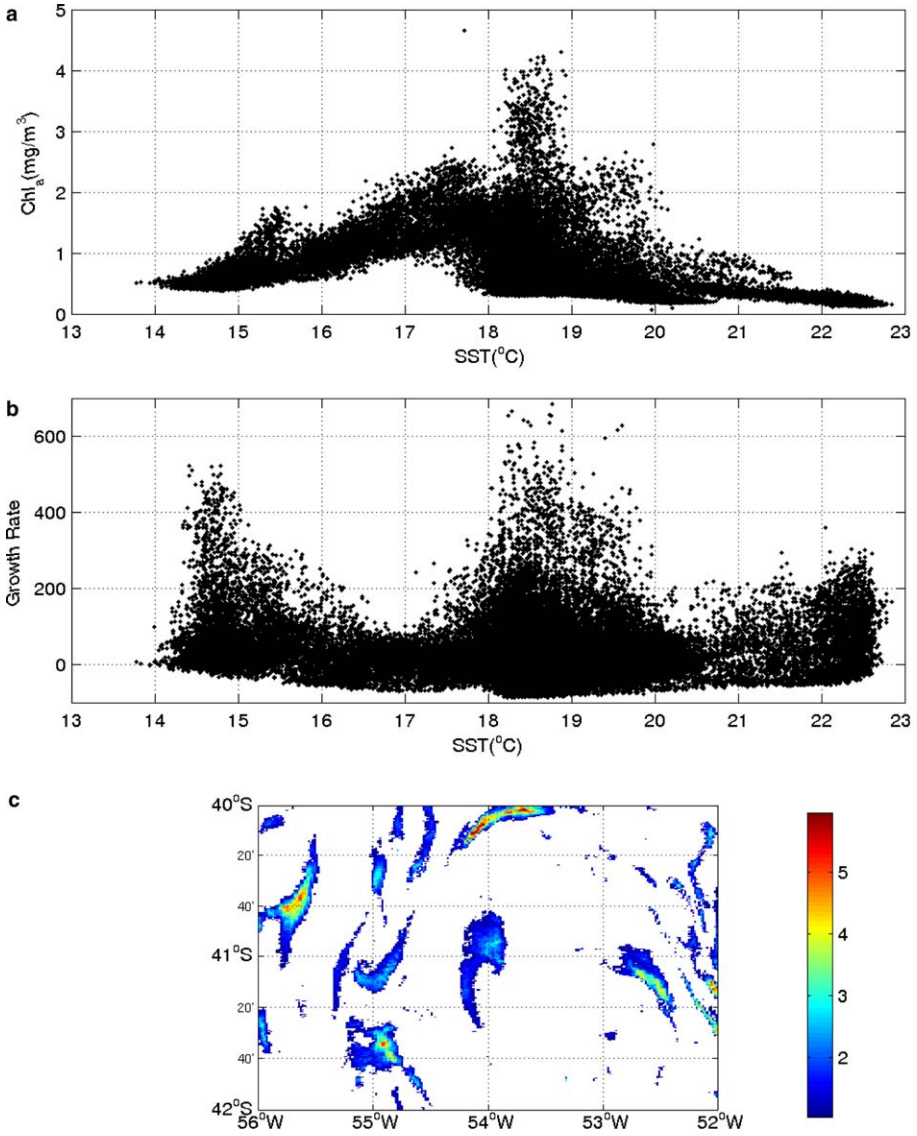

Fig. 12. (a) Scatter plot of Chl-*a* concentration as a function of temperature, on 5 March, 2004 (corresponding to Fig. 11(a)). (b) Apparent growth rate (computed as agr = (Chl-a_{t+1} − Chl-a_t)/Chl-a_t) as a function of temperature, on 5 March, 2004. (c) Spatial distribution of apparent growth rate: values less than 1 are blanked out. Colored values cannot be accounted for by local growth.

The chlorophyll-*a* sections exhibited maximum values in the region between the fronts in autumn, winter and spring: these maximum values varied from 0.8 mg/m^3 in autumn to 1.5 mg/m^3 in winter and to higher than 50 mg/m^3 in spring. These latter values clearly confirmed a continental-shelf origin for the surface water between the fronts.

In summer, the situation was totally different. The chlorophyll-*a* levels were very low (less than 0.2 g/m^3) over the BC, moderate in the region between the two thermal fronts (0.4 mg/m^3) and higher (close to 0.5 mg/m^3) over the MC. The summer chlorophyll-*a* image (Fig. 7) revealed that the MC was surrounded by high-chlorophyll-*a* water to the east and to the west and entrained filaments rich in chlorophyll-*a* from both sides. The chlorophyll-*a*-rich region to the west of the MC was associated with the Patagonian shelf break. This region has one of the longest (~1000 km) sustained high chlorophyll-*a* areas in the world ocean. Trapped coastal waves that induce a strong vertical circulation have been proposed as an explanation of this high-chlorophyll zone (Huthnance, 1995; Saraceno et al., 2005). The chlorophyll-*a*-rich region on the eastern side of the MC was associated with the Malvinas Return Flow (MRF). The high-chlorophyll-*a* area in the MRF occurred later in the year than that to the west of the MC (Saraceno et al., 2005). MODIS images suggested that it was at least partly due to advection of chlorophyll-*a*-rich shelf water by the B/M front. How much of the high chlorophyll-*a* concentration in the MRF was due to advection alone and how much was due to local production is an open question.

3.3.2.2. Meso- and sub-mesoscale structures downstream of the Brazil–Malvinas Current Confluence: an example from spring 2003. An enlargement of the region downstream of the B/M front in spring, when contrasts in chlorophyll-*a*

were maximum, showed that both SST and chlorophyll-*a* fields were thickly populated with features of a variety of structures and spatial scales (Fig. 10). Chlorophyll-*a* and SST exhibited similar patterns in the sense that the same coherent structures can be identified on both images. Chlorophyll-*a* and SST presented similar contours represented at first glance by the SST gradient. However, the relationship between SST and chlorophyll-*a* content varied from one structure to another. For example, structures with low chlorophyll-*a* concentration values corresponded to a wide range of temperatures. These chlorophyll-*a*-poor structures included: the cold (8 °C) Malvinas Current to the west; the core of the large (~100 km) temperate (14 °C) anticyclonic eddy to the southwest; the inner part of the elongated (~20 × 60 km) droplet-shaped warm (~24 °C) anticyclonic feature centered at 52.3°W, 39.7°S; the inner core of the cyclonic rather cold (~10 °C) small (~20 × 30 km) elliptical eddy centered at 51.8°W, 40.3°S, etc. By contrast, the striking filaments formed in the strain-dominated regions between eddies and/or along fronts had high values of chlorophyll-*a* (Fig. 10(d)). This high-resolution contrasted image documented the lateral mixing, the extension and the spiraling within or around the eddies. The SST distribution also exhibited a wealth of filaments documenting the lateral mixing. The largest chlorophyll-*a* filaments were surrounded by SST gradient maxima (Fig. 10(c)). As they became stirred, the filaments narrowed and the two SST maxima became indistinguishable. The width of the filaments was not directly related to their intensity, either in terms of chlorophyll-*a* or of SST, and deserves further examination.

The section corresponding to the image (Fig. 10) shows that the correspondence between the SST and chlorophyll-*a* is quite complex. We could distinguish the warm BC water (SST > 17 °C) and the cold MC water (SST < 7 °C) with low chlorophyll-*a* content at the extremities of the section north of 40.1°S and south of 41.9°S, respectively. In between was the temperate anticyclonic eddy core entraining spiraling filaments of cold and warm waters. The arrow-shaped high-chlorophyll-*a* structure centered at 52.8°W, 41.2°S was intriguing since it corresponded only partly to a gradient in SST. It suggested some kind of stagnation or accumulation point.

3.3.3. Short time-scales

To document variation in SST and chlorophyll-*a*, simultaneously at short time-scales, we examined two successive images (1 day apart) and computed their difference. We show one example for the austral summer (5–6 March, 2004) downstream of the B/M front, in the turbulent region to the southeast (Figs. 7(a) and 11). The selected images exhibited filamental structures rich in chlorophyll-*a* to the west, northeast and southeast, and a depleted region in the center (Fig. 11). The SST showed rather cold water to the west (14 °C), to the northeast and southeast corners (18 °C) and a warm patch in the center (up to 23 °C). In this small region (200 × 300 km), two water masses were identifiable on a Chl-*a*/SST scatter plot: modified water from the MC, with relatively cold water warmed up in summer (14 °C) and with a low chlorophyll-*a* content (0.5 mg/m^3), and warm water (18–22 °C) from the BC, with low chlorophyll-*a* concentration (0.2 mg/m^3; Fig. 12(a)). There was undoubtedly some water from the continental shelf, with intermediate temperature (18 °C) and an extremely high chlorophyll-*a* concentration (up to 4 mg/m^3; Fig. 12(a)). The high chlorophyll-*a* values (>2 mg/m^3) were present in the form of filaments and patchy structures (Fig. 11(a) and (b)).

The differences between the two successive chlorophyll-*a* fields and the two successive SST fields revealed remarkably similar spatial patterns and, in particular, an upside-down drop-like structure rich in chlorophyll-*a* and which cooled between the two days of observation (Fig. 11(c)). In 24 h, differences reached very high values, up to ±4 °C in SST, ±2 mg/m^3 in chlorophyll-*a*. Could these huge differences have a biological or physical origin or should they be considered as spurious?

An apparent growth rate (agr) was computed as

$$\mathrm{agr} = (\mathrm{Chl} - a_{t+1} - \mathrm{Chl} - a_t)/\mathrm{Chl} - a_t,$$

where t is time. The apparent growth rate varied from −90% to 700% (Fig. 12(b) and (c)), the latter value being far too large to have local biological production as a cause, and therefore indicative of other processes (e.g., advection). If we consider that a biological growth rate in excess of 100% in 24 h is not possible, then all the colored regions in Fig. 12(c) are subject to other processes than local growth.

The fact that temporal differences in SST and chlorophyll-*a* exhibit similar spatial structures (Fig. 11(c)) suggested links between variations in SST and in chlorophyll-*a*. A scatter plot of chlorophyll-*a* differences as a function of SST differences between the two images was somewhat disappointing and revealed only a very weak regression with the equation $Q = \Delta\text{Chl-}a + 0.0231\Delta\text{SST} + 0.1429$, where ΔChl-*a* is the chlorophyll-*a* concentration difference between the two successive images and ΔSST, the corresponding SST difference (Fig. 13(a)). We computed the quantity Q and blanked out the pixels for which Q was comprised between −1.46 and +1.46, values that corresponded to the 95%-confidence level on the scatter plot. The pixels that were not blanked out corresponded to the ones above and below the *red* lines of Fig. 13(a). They corresponded to variations in chlorophyll-*a* concentration that cannot be explained even by some very loose relation between SST and chlorophyll-*a*. Apart from the negative feature in the northeast corner, these structures, which cannot be explained by some weak relation with SST, cannot be explained by local biological growth or decay either: all corresponded to extreme values in Fig. 12(c) and to extreme positive values (>2 mg/m^3) on the 24-h chlorophyll-*a* difference (Fig. 11(c)).

We interpreted these large values as further proof that MODIS values above 2 mg/m^3 are problematic and, as a further confirmation, if necessary, that the high values downstream of the of the B/M front correspond to the continental shelf water.

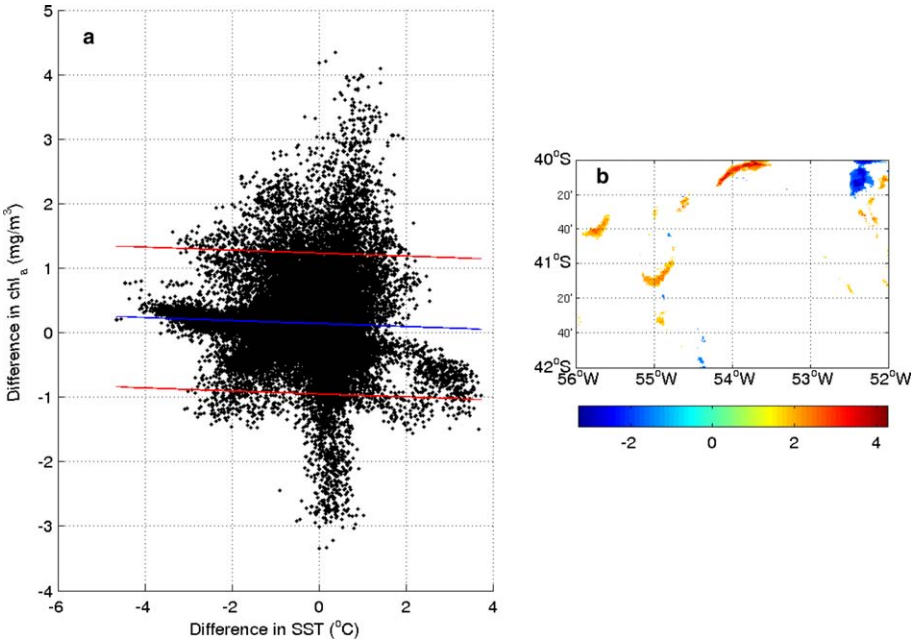

Fig. 13. (a) Scatter plot of ΔChl-*a* as a function of ΔSST where ΔChl-*a* is the Chl-*a* concentration difference between the two successive images of Fig. 11 and ΔSST the corresponding SST difference. The blue line corresponds to the regression line (equation $Q = \Delta\text{Chl-}a + 0.0231\Delta\text{SST} + 0.1429$). The red lines correspond to the 95% confidence interval on the scatter plot ($Q = \pm 1.46$). (b) Spatial distribution of the quantity Q. The pixels for which the absolute value of Q is less than 1.46 are blanked out. The colored pixels correspond to the points of the scatter diagram above or below the red lines.

4. Summary, discussion and perspectives

MODIS provides a remarkable data set with, for the first time, truly simultaneous daily SST and chlorophyll-*a* images with a 1.1-km resolution. Level-3 data, averaged weekly, from various sources (AMSR-E and MODIS for SST; SeaWiFS and MODIS for ocean color) were compared. Spatial distributions agreed very well. However, differences between MODIS and SeaWiFS chlorophyll-*a* concentrations are large in pigment-rich regions over the continental shelf.

MODIS data confirm the small variability of the location of the B/M front and its change in orientation from NS during most of the year, to NW–SE in summer. However, with this synoptic high-resolution data set, we could distinguish two SST gradients (i.e., two thermal fronts), one corresponding to the southernmost location of the BC, the other, the northernmost location of the MC. The two fronts remained close to each other (distance less than 100 km). The region between the two thermal fronts was a local maximum in chlorophyll-*a* concentration, corresponding to surface water from the continental shelf that is squeezed between the two fronts and entrained far from the coast.

MODIS documents in an unprecedented way the filaments in SST and surface chlorophyll-*a* concentration as they are stirred and stretched by meso- and sub-mesoscale structures in the strain-dominated region of the B/M front. Rough estimates of apparent growth rates from images one day apart are largely in excess of 100%, indicating that other processes are at work. Very high chlorophyll difference between the two consecutive daily images cannot be explained either by biological production or by physical processes linked with SST, and confirm that the high values in excess of 2 mg/m^3 in the MODIS data are not reliable and that the high-chlorophyll values downstream of the B/M front were probably of continental-shelf origin. It is suggested that a large part of the chlorophyll maximum associated with the MRF was due to the advection of water entrapped between the fronts of the Brazil Current and the Malvinas Current.

To discuss more quantitatively the part of variability due to the physical fields and the part that may be of biological origin, we intend to estimate the horizontal velocity field from two successive SST images using the method by Vigan et al. (2000). Then, using the SST-derived velocity field, we should be able to estimate the part of the chlorophyll-*a* variations due to advection, the sources and sinks of chlorophyll-*a*.

Simultaneous SST and chlorophyll-*a* data provided by MODIS offer great potential for examining meso- and sub-mesoscale structures and make progress on issues relative to patchiness, stirring and mixing (Abraham, 1998; Martin, 2003) and the role of meso- and sub-mesoscale dynamics on phytoplankton (e.g., Oschlies and Garçon, 1998; Garçon et al., 2001). However, one should not forget that the MODIS high-chlorophyll-*a* values are not reliable and that cloud cover is a strong constraint on the radiometric observations.

Acknowledgements

Our gratitude goes to Ray C. Griffiths for his valuable comments which helped clarify the present manuscript.

This work was supported by CNES (Centre National d'Etudes Spatiales).

References

Abraham, E.R. The generation of plankton patchiness by turbulent stirring. Nature 391, 577–580, 1998.

Agra, C., Nof, D. Collision and separation of boundary currents. Deep Sea Res., Part 1 40, 2259–2282, 1993.

Gan, J., Mysak, L.A., Straub, D.N. Simulation of the South Atlantic Ocean circulation and its seasonal variability. J. Geophys. Res. 103, 10241–10251, 1998.

Garçon, V.C., Oschlies, A., Doney, S.C., McGillicuddy, D., Waniek, J. The role of mesoscale variability on plankton dynamics in the North Atlantic. Deep-Sea Res II 48, 2199–2226, 2001.

Goni, G., Wainer, I. Investigation of the Brazil Current front dynamics from altimeter data. J. Geophys. Res. 106, 31117–31128, 2001.

Huthnance, J.M. Circulation, exchange and water masses at the ocean margin: the role of physical processes at the shelf edge. Prog. Oceanogr. 35 (4), 353–431, 1995.

Lebedev, I., Nof, D. The drifting Confluence zone. J. Phys. Oceanogr., 2429–2448, 1996.

Lebedev, I., Nof, D. Collision of boundary currents: beyond a steady state. Deep-Sea Res. 44, 771–791, 1997.

Matano, R.P. On the separation of the Brazil Current from the coast. J. Phys. Oceanogr. 23, 79–90, 1993.

Martin, A.P. Phytoplankton patchiness: the role of lateral stirring and mixing. Prog. Oceanogr. 57, 125–174, 2003.

Olson, D.B., Podesta, G.P., Evans, R.H., Brown, O.B. Temporal variations in the separation of the Brazil and Malvinas Currents. Deep Sea Res. 35, 1971–1990, 1988.

O'Reilly J., Maritorena, S., O'Brien, M., Siegel, D., Toole, D., Menzies, D., Smith, R., Mueller, J., Mitchell, B., Kahru, M., CHavez, F., Strutton, P., Cota, G., Hooker, S., McClain, C., Carder, K., Muller-Karger, F., Harding, L., Magnuson, A., Phinney, D., Moore, G., Aiken, J., Arrigo, K., Letelier, R., Culver, M. SeaWiFS Postlaunch Technical Report Series, vol. 11, SeaWiFS Postlaunch Calibration and Validation Analyses, Part 3, NASA Technical Memorandum, 2000.

Oschlies, A., Garçon, V. Eddy-induced enhancement of primary production in a model of the North Atlantic Ocean. Nature 394, 266–269, 1998.

Provost, C., Garcia, O., Garçon, V. Analysis of satellite sea surface temperature time series in the Brazil–Malvinas Current Confluence region: dominance of the annual and semi-annual periods. J. Geophys. Res. 97, 17841–17858, 1992.

Provost, C., Le Traon, P.-Y. Spatial and temporal scales in altimetric variability in the Brazil–Malvinas Confluence region: dominance of the semi-annual period and large spatial scales. J. Geophys. Res. 98, 18037–18051, 1993.

Provost, C., Gana, S., Garçon, V., Maamaatuaiahutapu, K., England, M. Hydrographic conditions during austral summer 1990 in the Brazil/Malvinas Confluence region. J. Geophys. Res. 100 (C6), 10655–10682, 1995.

Provost, C., Garçon, V., Medina Falcon, M. Hydrographic conditions in the surface layers over the slope-open ocean transition area near the Brazil–Malvinas Confluence during austral summer 1990. Cont. Shelf Res. 16, 215–235, 1996.

Saraceno, M., Provost, C., Piola, A.R., Bava, J., Gagliardini, A. Brazil–Malvinas frontal system as seen from years of advanced very high resolution radiometer data. J. Geophys. Res. 109, doi:10.1029/2003JC002127, 2004.

Saraceno, M., Provost, C., Piola, A.R. On the relationship of satellite retrieved surface temperature fronts and chlorophyll-*a* in the western South Atlantic. J. Geophys. Res., 2005 (in press).

Smith, L.T., Chassignet, E.P., Olson, D.B. Wind forced variations in the Brazil–Malvinas Confluence region as simulated in coarse resolution numerical model of the South Atlantic. J. Geophys. Res. 99, 5095–5117, 1994.

Vigan, X., Provost, C., Podesta, G. Sea surface velocities from sea surface temperature image sequences: 2. Application to the Brazil–Malvinas Confluence area. J. Geophys. Res. 105 (C8), 19515–19534, doi:10.1029/2000JC900028, 2000.

Vivier, F., Provost, C. Volume transport of the Malvinas Current: can the flow be monitored by TOPEX/Poseidon? J. Geophys. Res. 104, 21105–21122, 1999.

Werdel, P.J. Will SeaWiFS and MODIS/Aqua products be different if Lw(λ) is perfectly retrieved? Available from: http://oceancolor.gsfc.nasa.gov/DOCS/SeaWiFS_modis_diff.pdf, 2004.